

Magnetocrystalline Anisotropy in Permalloy Revisited

L. F. Yin, D. H. Wei, N. Lei, L. H. Zhou, C. S. Tian, G. S. Dong, and X. F. Jin*

Surface Physics Laboratory, Fudan University, Shanghai 200433, China

L. P. Guo and Q. J. Jia

Beijing Synchrotron Radiation Facility (BSRF), Beijing 100049, China

R. Q. Wu

Department of Physics and Astronomy, University of California at Irvine, Irvine, California 92697, USA

(Received 13 January 2006; published 9 August 2006)

Permalloy with a body-centered-cubic structure has been grown on GaAs(001) by molecular beam epitaxy. Its magnetism, Curie temperature, and magnetic anisotropy are determined experimentally and compared to those of conventional face-centered-cubic Permalloy. Unexpectedly the vanishing magnetic cubic anisotropy in Permalloy is found to be independent of its atomic structure but depends only upon the stoichiometry of Fe and Ni in the $\text{Fe}_x\text{Ni}_{1-x}$ alloy. This observation is further investigated and confirmed by first-principles electronic band calculations, which help to understand the long-standing issue of why Permalloy should be a soft magnet.

DOI: [10.1103/PhysRevLett.97.067203](https://doi.org/10.1103/PhysRevLett.97.067203)

PACS numbers: 75.30.Gw, 31.15.Ar, 75.50.Bb, 78.20.Ls

$\text{Fe}_x\text{Ni}_{1-x}$ alloys under ambient conditions adopt either the bcc structure at the Fe-rich side or the fcc structure at the Ni-rich side with a borderline at the stoichiometry of $x \approx 0.65$. Permalloy (Py) usually refers to $\text{Fe}_x\text{Ni}_{1-x}$ alloys in the fcc phase with a stoichiometry of $0.18 \leq x \leq 0.25$ that have a vanishingly small magnetocrystalline anisotropy and magnetostriction but extremely large magnetic permeability. These unique properties make Py one of the most important soft magnets in a variety of exploitations, such as the cores of motors and the free layers of spin-valve magnetic reading heads. However, it is still unclear from the fundamental point of view why the magnetic cubic anisotropy energy of Py should be so small, while both Fe and Ni have large magnetic anisotropy energy, i.e., $K_1^{\text{Fe}} = +4.7 \times 10^5 \text{ erg} \cdot \text{cm}^{-3}$ and $K_1^{\text{Ni}} = -5.7 \times 10^4 \text{ erg} \cdot \text{cm}^{-3}$ at room temperature [1]. Here, positive K_1 means that the magnetic easy axis is along $\langle 100 \rangle$, the hard axis is along $\langle 111 \rangle$, and vice versa. In addition to the fundamental importance, a better understanding about the vanishing magnetic anisotropy in Py is crucial for the rational design of innovative intermetallic materials for various applications.

It has long been believed that the vanishing of K_1 in Py stems from the cancellation between the positive K_1 of Fe and the negative K_1 of Ni [1], a conjecture which was first proposed by Mckeehan with the atomic spin model [2] and later explained qualitatively by Brooks with the tight binding itinerant electron model [3]. This cancellation picture works surprisingly well for the interpretation of the magnetic anisotropy phase diagram of $\text{Fe}_x\text{Ni}_{1-x}$ alloys [4,5], and was even used to support findings of some recent first-principles calculations [6,7]. However, the following are still unclear at present: (1) whether the vanishing K_1 is an accidental event in the fcc structure of $\text{Fe}_x\text{Ni}_{1-x}$, presum-

ably driven by the different tendencies from Ni and Fe; (2) whether Fe and Ni atoms in $\text{Fe}_x\text{Ni}_{1-x}$ alloys with other structures also show the same tendencies to the magnetic anisotropy as in their bulks, the root of the cancellation model; (3) what would happen if K_1 of both constituents are large and have the same sign.

In this Letter, we strive to address these challenging issues through synergistic experimental and theoretical investigations. It was demonstrated that bcc Ni has a positive K_1 , $+4.0 \times 10^5 \text{ erg} \cdot \text{cm}^{-3}$ at room temperature [8]. According to the standard cancellation model, bcc $\text{Fe}_x\text{Ni}_{1-x}$ would have a large positive K_1 because both contribute positively. Here, we report successful synthesis of bcc Py on GaAs(001) by molecular beam epitaxy at 200 K. Strikingly, bcc Py also displays vanishingly small cubic magnetocrystalline anisotropy at $x \approx 0.25$, which directly challenges the standard cancellation model. Our first-principles calculations confirmed the trend of experimental observations and helped to establish a more transparent picture for magnetic anisotropy in intermetallic alloys, essential for tailoring the magnetic anisotropic energy for practical applications.

Since both Fe [9] and Ni [8] grow epitaxially on GaAs(001) in the bcc structure, one would anticipate that $\text{Fe}_x\text{Ni}_{1-x}$ alloys also adopt the bcc structure on GaAs(001). The growth was done at 200 K with the codeposition method in a molecular beam epitaxy chamber with multi-technique approach *in situ*. Representative low energy electron diffraction (LEED) and reflection high energy electron diffraction (RHEED) patterns in Fig. 1 show that $\text{Fe}_x\text{Ni}_{1-x}$ films are in a high quality single crystalline bcc structure on GaAs(001). Figure 1(a) clearly shows the LEED pattern of the (4×6) reconstructed clean GaAs(001) surface. The sharp LEED spots and RHEED

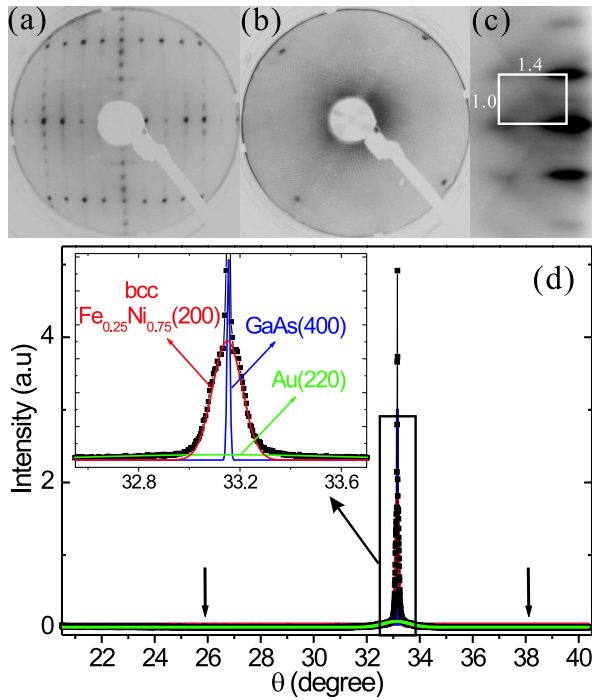


FIG. 1 (color online). (a),(b) LEED ($E = 57$ eV) patterns for GaAs(001)-(4 \times 6) and 0.8 nm bcc Py on it. (c) RHEED pattern for 1 nm thick bcc Py on GaAs(001), with the incident electron along the $[1\bar{1}0]$ direction. (d) GIXRD spectrum with incident angle at 0.3° for 5 nm Py, fitted by three identified peaks as in the text. The absence of peaks at 25.9° and 38.1° shows the absence of fcc Py.

lines in Figs. 1(b) and 1(c) and the spacing between them unambiguously indicate the bcc morphology of the $\text{Fe}_{0.25}\text{Ni}_{0.75}$ film, similar to what was observed for bcc Fe and Ni films grown on the same substrate [10].

To further verify the bcc structure, we also conducted the grazing incident x-ray diffraction (GIXRD) measurement at the Beijing Synchrotron Radiation Facility. Before taking the samples out of the vacuum chamber, a 2-nm Au capping layer was deposited on the 5-nm $\text{Fe}_{0.25}\text{Ni}_{0.75}$ film. Figure 1(d) presents a GIXRD spectrum of the (2 nm)Au/(5 nm)Py/GaAs(001) sample with a fixed photon energy at 8.052 keV and an incident angle at 0.3° . First, it is clear that Py film prepared on GaAs(001) is not fcc since no signal is observed at 25.9° and 38.1° for fcc Py(200) and Py(220), positions indicated by the two arrows. The main peak observed at 33.1° comes from three different contributions as indicated by three arrows in the inset: (I) an extremely narrow peak at 33.155° with 0.014° full width at half maximum (FWHM) from the GaAs(400) diffraction as shown in blue line in the inset; (II) a broad peak with $\text{FWHM} \approx 0.15^\circ$ from the bcc-Py(200) diffraction with an in-plane lattice constant of 0.2825 nm as shown by the red line; (III) a very broad and shallow peak with $\text{FWHM} \approx 1.2^\circ$ from the fcc-Au(220) diffraction of the capping layer as shown in the green line. The messages from Fig. 1 are consistent and undoubtedly in-

dicating that Py grown on GaAs(001) at 200 K adopts the bcc structure. It should also be pointed out that similar results are obtained for samples with other compositions. We hence believe that $\text{Fe}_x\text{Ni}_{1-x}$ grow in the bcc structure on GaAs(001) for the whole range of stoichiometry.

To explore the magnetic properties of bcc Py, *in situ* investigations were carried out through both longitudinal and polar magneto-optical Kerr effect (MOKE) measurements at 110 K. For highly reliable comparisons, fcc and bcc Py were prepared on the same sample as shown in the inset of Fig. 2(a). The right half of the GaAs(001) sample was initially blocked by a shadow mask, and the left half of the sample was covered at room temperature by a 3 nm thick epitaxially grown fcc-Au seed layer [11]. Then the shadow mask was removed and a thickness wedge of Py was deposited on the whole sample in the way shown in the figure. Since Py grows on fcc Au in the fcc phase while on GaAs in the bcc phase, this special sample has fcc and bcc Py side by side with exactly the same stoichiometry and thickness along the wedge.

It is found in experiments that all the films in either fcc or bcc have the easy in-plane magnetization; therefore only

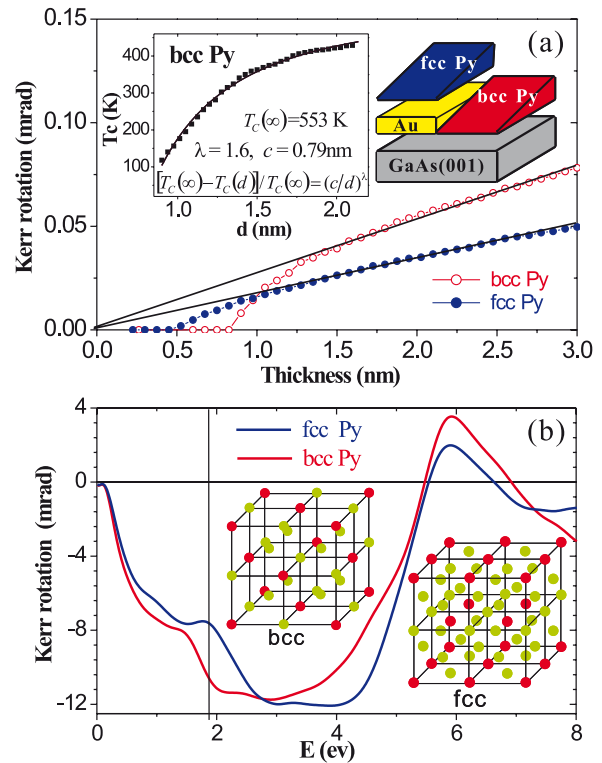


FIG. 2 (color online). (a) Kerr rotations of bcc and fcc $\text{Fe}_{0.25}\text{Ni}_{0.75}$ as a function of film thickness. The right inset shows the special sample prepared for this measurement. The left inset gives the finite size scaling of the Curie temperature of the bcc-Py film; dots for experimental data and line for the fitting. (b) Calculated Kerr rotations of fcc and bcc $\text{Fe}_4\text{Ni}_{12}$. The solid line at 1.85 eV corresponds to the laser wavelength used in experiment. The insets give the supercells adopted for bcc and fcc Py.

longitudinal MOKE data at saturation will be discussed henceforth. Interestingly, the slopes of Kerr rotations versus thickness in Fig. 2(a) are distinctly different between bcc Py and fcc Py. Unambiguously, we found that the apparent MOKE difference is caused by the optical effect, because vibrating sample magnetometer (VSM) measurements on the corresponding flat fcc- and bcc-Py samples indicate that the magnetic moments per atom are almost identical for bcc and fcc Py: $m_{\text{bcc}} = 1.03 \pm 0.09 \mu_B$ and $m_{\text{fcc}} = 1.07 \pm 0.09 \mu_B$. The latter agrees well with the existing data [12].

Besides the magnetization, it is also essential to measure the Curie temperature of the new bcc Py. As was established, the Curie temperature in an ultrathin film increases with its thickness [8,13,14]. To extract the bulk Curie temperature, we measured the Curie temperature as a function of film thickness in a wedged bcc-Py film, as shown in the inset of Fig. 2(a). It was found that $T_c = 553$ K for the bulk bcc Py. This is significantly lower than $T_c = 871$ K for the bulk fcc Py [15], and the difference can be understood by first-principles calculations together with Monte Carlo simulations (will be discussed elsewhere).

We further examined the in-plane (cubic) magnetic anisotropy of the new bcc Py with *ex situ* longitudinal MOKE on the special sample with half bcc Py and half fcc Py mentioned above, capped with 2 nm thick Au overlayer on the whole sample before taking it out of the vacuum chamber. The top left inset of Fig. 3 shows the result corresponding to (2 nm)Au/(3 nm)bcc-Py/GaAs(001). Surprisingly, except a small uniaxial magnetic anisotropy caused by the substrate as generally found for 3d magnetic metals on III-V semiconductors [16], the cubic magnetic

anisotropy is extremely small, very similar to the results of (2 nm)Au/(3 nm)fcc-Py/(3 nm)Au/GaAs(001) (not shown here). In order to address the issue more quantitatively, we proceed to prepare another very special sample—the so called composition wedge of bcc $\text{Fe}_x\text{Ni}_{1-x}$ on GaAs(001) as shown by the carton in Fig. 3 (a detailed description will be published elsewhere [17]). Four composition wedge samples were prepared to bridge the entire stoichiometry range of $\text{Fe}_x\text{Ni}_{1-x}$. With the well-established longitudinal MOKE combined with a rotating magnetic field, i.e., the ROTMOKE or vector MOKE technique [8,18,19], we obtained the cubic magnetic anisotropy, K_1 , at room temperature for the whole range of compositions, as shown in Fig. 3. Strikingly, the $K_1(x)$ curve shows a tublike line shape, which is completely different from that of fcc $\text{Fe}_x\text{Ni}_{1-x}$ for which the $K_1(x)$ curve starts from positive at the Fe-rich side, passes through zero (at 25% Fe), and becomes negative at the Ni-rich side. To ensure that data in Fig. 3 are intrinsic for the bulklike Py, we carefully checked the effects of film thickness and Au capping. It was found that K_1 reached its asymptote, also stable in 110–300 K, when the films are 2.5 nm thick. The $M(H)$ curves of bcc Py measured *in situ* show no noticeable line shape change besides the anticipated attenuation of the MOKE intensity, before and after the 2 nm Au capping.

Furthermore, it is seen in the top right inset of Fig. 3 that the magnetization versus concentration curve of bcc $\text{Fe}_x\text{Ni}_{1-x}$ on GaAs(001) measured by VSM on the flat film samples obeys very well the Slater-Pauling behavior, showing no traces of the high-spin to low-spin transition as observed in the fcc $\text{Fe}_x\text{Ni}_{1-x}$ alloy on Cu(001) [20]. Finally, it is observed in the same inset that the magnetization of bcc $\text{Fe}_x\text{Ni}_{1-x}$ measured by MOKE has nothing peculiar nearby the eminent “Invar point” (65% Fe), where the fcc-bcc structural phase transition happens in the conventional bulk $\text{Fe}_x\text{Ni}_{1-x}$ alloy.

To understand the striking properties observed, we carried out first-principles calculations using the full potential linearized augmented plane wave method [21] in conjunction with the generalized gradient approximation (GGA) [22]. When $x = 0.25$, with the $(2 \times 2 \times 2)$ supercells shown in the inset of Fig. 2(b), the calculated spin magnetic moments for bcc and fcc-Py are $m_{\text{bcc}} = 1.11 \mu_B/\text{atom}$ and $m_{\text{fcc}} = 1.14 \mu_B/\text{atom}$, respectively. These results are in good accordance with the VSM data listed above. Since the calculations were done in a chemically ordered supercell (e.g., the DO_3 structure for the bcc lattice), the chemical disordering in experimental samples appears to be not important for the magnetization [23]. To explain the discrepancy between the observed magnetic moments determined by the Kerr rotations for the bcc and fcc Py, we calculated their MOKE spectra in a wide range of photon energy and the results are shown in Fig. 2(b). At the photon energy of red laser ($\lambda = 670$ nm, denoted by the vertical line to guide the eye), bcc Py shows 1.4 times larger Kerr

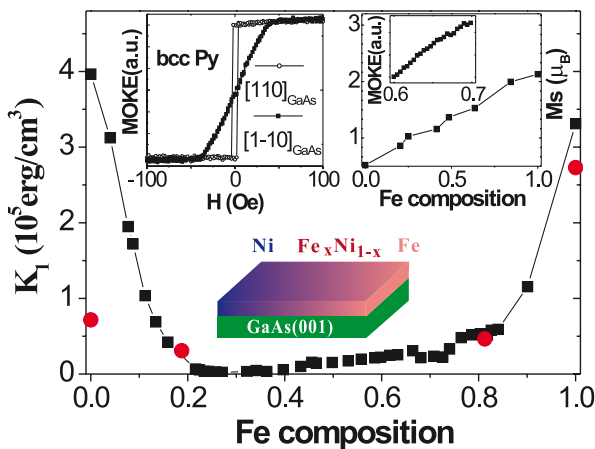


FIG. 3 (color online). Cubic magnetic anisotropy constant (K_1) versus iron concentration measured from 3 nm thick bcc $\text{Fe}_x\text{Ni}_{1-x}$ composition wedge (see the carton) by ROTMOKE at 300 K, together with the calculated K_1 values are marked as red solid circles. A set of representative hysteresis loops for bcc $\text{Fe}_{0.25}\text{Ni}_{0.75}$ is shown in the inset. Averaged magnetic moment per atom in bcc $\text{Fe}_x\text{Ni}_{1-x}$ is also measured by VSM as a function of iron concentration together with a zoomed in range around the “Invar point” obtained by MOKE.

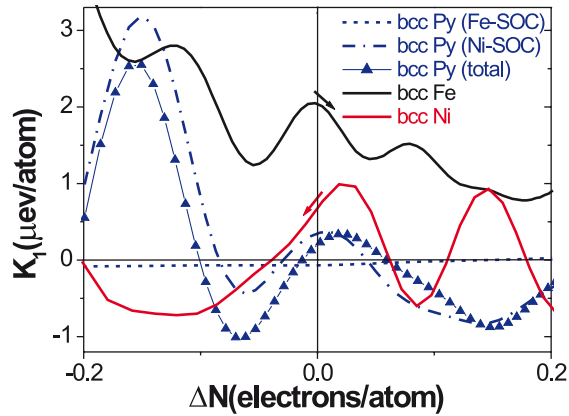


FIG. 4 (color online). Calculated K_1 of Fe, Ni, and $\text{Fe}_3\text{Ni}_{13}$ as a function of band filling. The vertical line at zero corresponds to the Fermi energy. “Fe-SOC” means only spin-orbit coupling of Fe is included and vice versa.

rotation than the fcc one, which confirms the experimental finding.

The cubic magnetocrystalline anisotropy energies were calculated through the torque method [24] for bcc $\text{Fe}_x\text{Ni}_{1-x}$ in several $(2 \times 2 \times 2)$ supercells that preserve the cubic symmetry. We used 13 824 k points in the first Brillouin zone to evaluate the integrals in the reciprocal space. The results are presented as dots in Fig. 3 for direct comparison with the experiment. It is obvious that theory reproduces well the general trend of the experimental data. The only inferior point is for the pure bcc Ni, primarily caused by the incorrect s - d charge transfer produced in GGA calculations as we discussed previously for fcc Ni [24]. The band-filling dependence of K_1 obtained from a rigid band scheme are presented in Fig. 4 for several systems. It is clear to see that adding either a small amount of Fe to Ni or vice versa causes reduction in K_1 as guided by the arrows. To elucidate the element specific contributions from Fe and Ni, we selectively switch off spin-orbit coupling (SOC) from different elements in the bcc Py. Intriguingly, the SOC of Fe only (denoted as Fe-SOC) gives a small negative contribution to K_1 whereas Ni plays the dominant role. Both Ni and Fe behave very differently from their bulk forms. This is not a surprise since the chemical environment is drastically different. For instance, the local magnetic moment of Fe is enhanced by about 30% to $2.88\mu_B$. Meanwhile, the spin magnetic moments of neighboring Ni are reduced to $0.35\mu_B$. It seems that only the local Fe-Ni bonding is the most important factor for the quenching of the magnitude of K_1 , whereas signs of K_1 of individual constituents are not relevant.

In conclusion, bcc-Py films were successfully fabricated on GaAs(001) and their structural and magnetic properties were carefully characterized using various techniques. We found that it is the charge redistribution that leads to the vanishing K_1 of Py in both fcc and bcc structures. Fe gives

negative contribution to K_1 of bcc Py, although K_1 in its bulk is positive. It is possible to design and synthesize soft magnets in binary alloys even if K_1 of both constituents are large and have the same sign.

This work was supported by the National Natural Science Foundation of China, the 973 Project of the Science and Technology Ministry of China, the Ministry of Education of China for Ph.D. Training, and the Shanghai Science and Technology Committee. R. Q. W. also acknowledges support from DOE.

*To whom correspondence should be addressed.

Electronic address: xfjin@fudan.edu.cn

- [1] See, for example, Derek Craik, *Magnetism: Principles and Applications* (John Wiley and Sons, Chichester, 1995), p. 392.
- [2] L. W. McKeehan, *Phys. Rev.* **52**, 18 (1937).
- [3] H. Brooks, *Phys. Rev.* **58**, 909 (1940).
- [4] L. P. Tarasov, *Phys. Rev.* **56**, 1245 (1939).
- [5] R. M. Bozorth, *Rev. Mod. Phys.* **25**, 42 (1953).
- [6] P. James, O. Eriksson, O. Hjortstam, B. Johansson, and L. Nordstrom, *Appl. Phys. Lett.* **76**, 915 (2000).
- [7] P. Weinberger, L. Szunyogh, C. Blaas, C. Sommers, and P. Entel, *Phys. Rev. B* **63**, 094417 (2001).
- [8] C. S. Tian *et al.*, *Phys. Rev. Lett.* **94**, 137210 (2005).
- [9] J. J. Krebs, B. T. Jonker, and G. A. Prinz, *J. Appl. Phys.* **61**, 2596 (1987).
- [10] W. X. Tang *et al.*, *J. Magn. Magn. Mater.* **240**, 404 (2002).
- [11] D. Y. Noh, Y. Hwu, H. K. Kim, and M. Hong, *Phys. Rev. B* **51**, 4441 (1995); T. G. Andersson, G. Le Lay, J. Kanski, and S. P. Svensson, *Phys. Rev. B* **36**, 6231 (1987).
- [12] Soshin Chikazumi, *Physics of Ferromagnetism* (Oxford University Press, New York, 1997).
- [13] See, for example, Renjun Zhang and Roy F. Willis, *Phys. Rev. Lett.* **86**, 2665 (2001).
- [14] B. Schulz, R. Schwarzwald, and K. Baberschke, *Surf. Sci.* **307–309**, 1102 (1994).
- [15] R. J. Wakelin and E. L. Yates, *Proc. Phys. Soc. London, Sect. B* **66**, 221 (1953).
- [16] G. Wastlbauer and J. A. C. Bland, *Adv. Phys.* **54**, 137 (2005).
- [17] C. S. Tian *et al.* (to be published).
- [18] Z. Tian *et al.*, *Phys. Rev. B* **70**, 012301 (2004).
- [19] R. Mattheis and G. Quednau, *J. Magn. Magn. Mater.* **205**, 143 (1999).
- [20] F. O. Schumann, R. F. Willis, K. G. Goodman, and J. G. Tobin, *Phys. Rev. Lett.* **79**, 5166 (1997).
- [21] E. Wimmer, H. Krakauer, M. Weinert, and A. J. Freeman, *Phys. Rev. B* **24**, 864 (1981); M. Weinert, E. Wimmer, and A. J. Freeman, *Phys. Rev. B* **26**, 4571 (1982).
- [22] J. P. Perdew, K. Burke, and M. Ernzerhof, *Phys. Rev. Lett.* **77**, 3865 (1996).
- [23] C. G. Shull and M. K. Wilkinson, *Phys. Rev.* **97**, 304 (1955).
- [24] R. Q. Wu and A. J. Freeman, *J. Magn. Magn. Mater.* **200**, 498 (1999).